N95-21765

115

395767

TWO-DIMENSIONAL MAPS OF THE INFRARED-TO-RADIO RATIO IN SPIRAL GALAXIES

KENNETH A. MARSH[1] AND GEORGE HELOU
Infrared Processing and Analysis Center, MS 100-22
California Institute of Technology, Jet Propulsion Laboratory
Pasadena, CA 91125

ABSTRACT We have produced two-dimensional maps of the intensity ratio Q_{60} of 60 μm infrared to 20 cm radio continuum emission, for a set of 25 nearby galaxies, mostly spirals. The ratio maps were obtained from infrared images made using Infrared Astronomical Satellite (IRAS) data with the Maximum Correlation Method, and radio images made using VLA data. Before taking the ratio, the radio images were processed so as to have the same resolution properties as the infrared images; the final spatial resolution in all cases is approximately 1′, corresponding to 1–2 kpc for most galaxies. These images allow us to study the variations of the Q_{60} ratio with unprecedented spatial resolution, and thus represent a major improvement over earlier work.

Our new high-resolution maps confirm the slow decrease of Q_{60} with increasing radial distance from the nucleus, but show additional structure which is probably associated with separate sites of active star formation in the spiral arms. The maps show Q_{60} to be more closely related to infrared surface brightness than to the radial distance in the galaxy disk. We expect that the results will provide improved constraints on the evolution (diffusion, decay and escape) of cosmic-ray electrons in the magnetic field of the disks.

INTRODUCTION

The strong correlation, observed in spiral galaxies, between flux densities at far-infrared and centimeter wavelengths (Helou, Soifer, and Rowan-Robinson 1985) has prompted comparisons between the spatial structure in these two wavelength regimes. In a recent study, Bicay and Helou (1990) compared the spatial distributions, at 60 μm and 20 cm wavelength, for 25 galaxies (24 late-type spirals and one irregular). They found that the radio images had the appearance of smeared versions of the infrared images, and that the smearing could be understood in terms of the diffusion of cosmic ray electrons. In their model, discussed in more detail by Helou and Bicay (1993), the correlation between infrared and radio emission is driven by massive stars heating up the dust, and causing cosmic-ray electrons to be accelerated during the supernova phase; the cosmic rays then give

[1] Jet Propulsion Laboratory 306-451, 4800 Oak Grove Drive, Pasadena, CA 91109

S. Terebey and J. Mazzarella (eds.), *Science with High-Spatial Resolution Far Infrared Data*, 115–120, 1994, Jet Propulsion Laboratory, Pasadena, CA.

PRECEDING PAGE BLANK NOT FILMED

rise to synchrotron radio emission which dominates at 20 cm. The difference in spatial distribution between infrared and radio arises because cosmic rays diffuse up to a few kpc before being lost to radiative decay or escape.

Bicay and Helou (1990) used the raw detector data from the Infrared Astronomy Satellite (IRAS), which are of rather coarse spatial resolution ($1.5' \times 4.7'$). Since the latter dimension was comparable to the sizes of the galaxies themselves, the study was basically one-dimensional in terms of spatial structure. In this paper we describe an improved approach to the same question using infrared data of higher spatial resolution ($\sim 1'$ in both coordinates).

DATA

The galaxy sample used in the current investigation consisted of the same 25 galaxies studied by Bicay and Helou (1990). Our input data for each galaxy consisted of:

(1) Radio continuum image at 20 cm wavelength (frequency 1.49 GHz) made using the VLA, and described by Condon (1987). The CLEAN algorithm was used for deconvolution, with circular Gaussian restoring beams of FWHM $0.8'$, $0.9'$, or $1.0'$.

(2) Infrared continuum image at 60 μm wavelength, made using data from the Infrared Astronomy Satellite (IRAS), and the imaging technique known as the Maximum Correlation Method (MCM), described by Aumann, Fowler, and Melnyk (1990). The number of iterations used was 20.

Although the infrared and radio images had comparable spatial resolution ($\sim 1'$), the infrared images were nonisoplanatic. The behavior of their resulting point spread functions (PSF) was determined by the IRAS scanning geometry, the spatial responses of the set of IRAS detectors, and the inherent properties of the MCM. Since the goal of the study was to compare radio and infrared images at the same spatial resolution, further processing was necessary.

ANALYSIS PROCEDURE

In order to produce pairs of images (radio and infrared) with the same spatial resolution, we re-CLEANed the radio images and restored them using an effective PSF corresponding to the infrared images. The procedure involved the following steps:

(1) Deconvolve the radio PSF. This step was necessary since the original sets of CLEAN components involved in Condon's (1987) maps were not available. The deconvolution was performed by a reapplication of the CLEAN algorithm, based on the same circular Gaussian beam which Condon had used to restore each map. The image was CLEANed down to the residual noise level (0.1 mJy/beam), yielding a source model in the form of a set of delta-function components.

(2) Generate synthetic "raw detector data" as would be observed if this source model were scanned using detectors whose spatial responses were the same as for IRAS, and using the same scanning geometry as for the original IRAS observations.

(3) Run these data through the same MCM imaging algorithm as was used to generate the infrared images. The pixel size (15″), field of view, and position of the center pixel, were the same as for the corresponding infrared image.

The result in each case was a radio image with spatial resolution properties similar to that of the infrared image.

Because of uncertainties in the absolute positioning of the IRAS data (resulting in errors comparable to a pixel width in the infrared images), it was necessary to perform a final registration step. The required position offset of the infrared image, $(\Delta\alpha,\Delta\delta)$, was estimated by minimizing the sum of squares of residuals, $\phi(\Delta\alpha, \Delta\delta, q)$, defined by:

$$\phi(\Delta\alpha, \Delta\delta, q) = \sum_{\alpha,\delta}[I_{20\mathrm{cm}}(\alpha, \delta) - q^{-1} I_{60}(\alpha - \Delta\alpha,\ \delta - \Delta\delta)]^2 \qquad (1)$$

where $I_{20\mathrm{cm}}(\alpha, \delta)$ and $I_{60}(\alpha, \delta)$ represent the intensity distributions at wavelengths 20 cm and 60 μm, respectively, as a function of right ascension, α, and declination, δ, and q is a scaling factor representing the weighted-mean ratio of infrared to radio intensity. The summation was performed over all positions which fell within a rectangular box, constructed so as to include the galaxy but exclude background sources.

The final numerical step was to calculate the infrared-to-radio intensity ratio, $Q_{60} = I_{60}/I_{20\mathrm{cm}}$, as a function of position. This quantity was then plotted, in the form of a greyscale image, for all positions for which $Q_{60} \geq 3\sigma_Q$, where σ_Q is the standard deviation in Q. The quantity σ_Q was determined by the noise levels in the infrared and radio images, which were dominated by the dynamic ranges of the processed radio maps, typically 70:1.

RESULTS

Figure 1 shows the results for three sample cases, namely NGC 5194, NGC 5236, and NGC 6946.

We have compared all 25 ratio maps with the corresponding infrared intensity maps, and find that in nearly all cases, there is a local maximum in Q_{60} coincident with the galactic nucleus, and that the average Q_{60} in an annulus centered on the nucleus decreases monotonically with radial distance, r, from the nucleus, in a manner which is in qualitative agreement with the Bicay and Helou (1990) model. The principal exceptions to this behavior were IC 10 (an irregular galaxy) and NGC 3031 (a disk galaxy with a strong Seyfert nucleus), neither of which were expected to fit the model.

In addition to the general radial behavior of Q_{60} described above, the improved spatial resolution reveals in some galaxies off-nucleus local maxima in Q_{60}, which coincide with local maxima in I_{60}. These new details are seen in the well-resolved face-on spirals, and are particularly prominent in NGC 5194, NGC 5236, and NGC 6946. They also appear in the edge-on spiral, NGC 4631. These local maxima correspond to locally prominent star formation regions in the spiral arms. The new features cannot be accounted for in the simple model by Helou and Bicay (1993), which describes the I_{60} distribution as an exponential disk. They therefore partially destroy the predicted gradient of Q_{60} as a

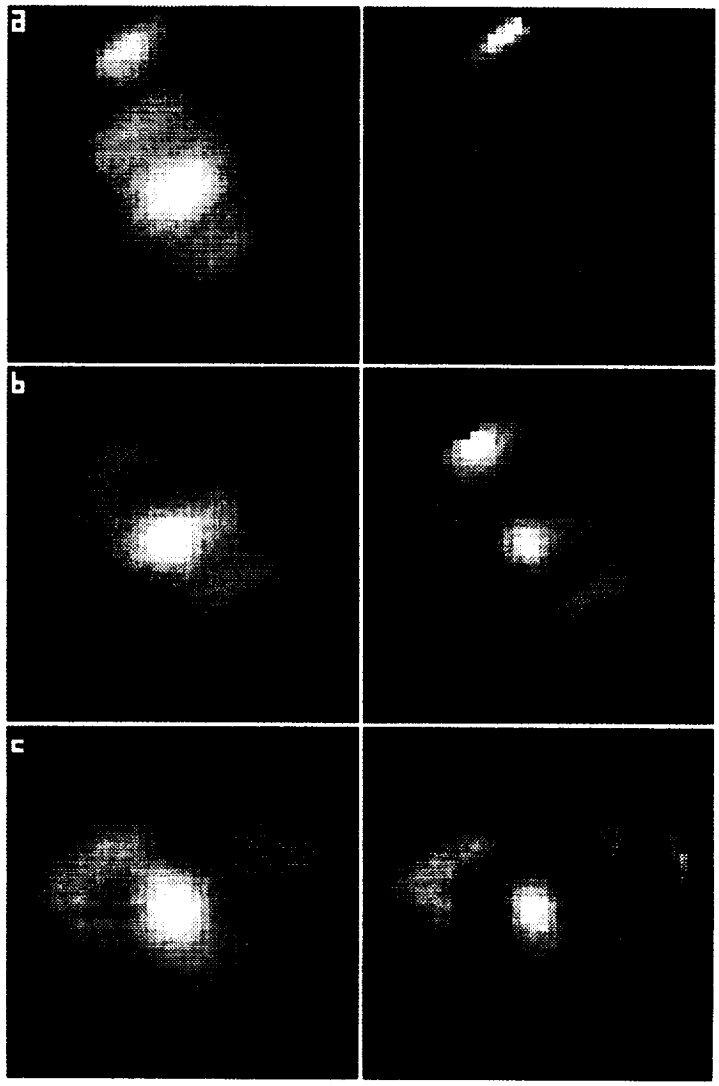

FIGURE 1 Maps of 60 μm infrared surface brightness, presented on a logarithmic scale of 2.5 decades (left hand plots) and the intensity ratio of 60 μm infrared to 20 cm radio emission, presented on a linear scale (right hand plots). The field of view in all cases is $16' \times 16'$. (a) NGC 5194 (Peak value of ratio map = 284); (b) NGC 5236 (Peak value of ratio map = 266); (c) NGC 6946 (Peak value of ratio map = 220).

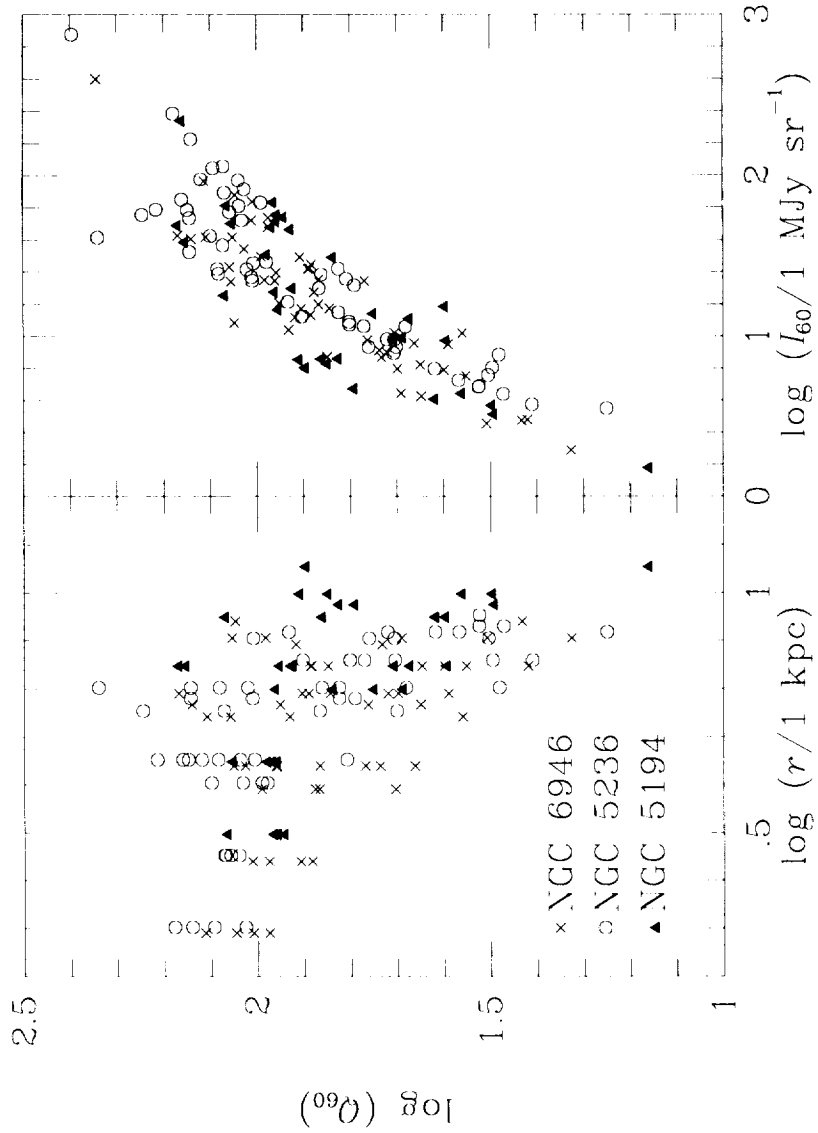

FIGURE 2 Scatter plots of Q_{60} as a function of radial distance from nucleus, r, and infrared surface brightness, I_{60}, for NGC 5194, NGC 5236, and NGC 6946.

function of r. This is clearly visible in Figure 2, which shows scatter plots of Q_{60} *vs.* r for NGC 5194, 5236 and 6946.

The essential content, however, of the Bicay and Helou model is not in the geometry, but in the physics of diffusion, escape and decay of cosmic-ray electrons, and the effects on the appearance of the radio map. These effects should apply locally to each center of star formation activity, and cause the ratio Q_{60} to fall with increasing distance from each center. Since I_{60} also falls with increasing distance from a center of activity, one would expect Q_{60} and I_{60} to be positively correlated. We test this hypothesis using scatter plots of Q_{60} v. r and Q_{60} v. I_{60}. The results for NGC 5194, NGC 5236, and NGC 6946 are shown in Figure 2. The three plots are clearly consistent with our expectations, i.e., Q_{60} is more closely related to infrared surface brightness than to the radial distance in the galaxy disk.

In a forthcoming paper we will present the complete results for all 25 galaxies in the sample, and discuss the physical constraints that these results impose on the evolution of cosmic rays in the magnetic field of the disks.

ACKNOWLEDGMENTS

We acknowledge stimulating discussions with M. D. Bicay and Zhong Wang. We thank Diane Engler for running the MCM software. This research has been supported through the IRAS Extended Mission Program by the Jet Propulsion Laboratory, California Institute of Technology, under contract with the National Aeronautics and Space Administration.

REFERENCES

Aumann, H. H., Fowler, J. W. and Melnyk, M. 1990, *AJ* **99**, 1674

Bicay, M. D. and Helou, G. 1990, *Ap. J.* **362**, 59

Condon, J. J. 1987, *Ap. J. (Suppl.)* **65**, 485

Helou, G. and Bicay, M. D. B. 1993, *Ap. J.* (in press)

Helou, G., Soifer, B. T. and Rowan-Robinson, M. 1985, *Ap. J.* **298**, L7